Bioorganic & Medicinal Chemistry 19 (2011) 1072–1078

Contents lists available at ScienceDirect

Bioorganic & Medicinal Chemistry

journal homepage: www.elsevier.com/locate/bmc

Design and synthesis of a novel fluorescence probe for Zn^{2+} based on the spirolactam ring-opening process of rhodamine derivatives

Hiromi Sasaki [a,b], Kenjiro Hanaoka [a,b], Yasuteru Urano [a], Takuya Terai [a,b], Tetsuo Nagano [a,b,*]

[a] Graduate School of Pharmaceutical Sciences, The University of Tokyo, 7-3-1, Hongo, Bunkyo-ku, Tokyo 113-0033, Japan
[b] CREST, Japan Science and Technology Agency, Kawaguchi Center Building, 4-1-8, Honcho, Kawaguchi-shi, Saitama 332-0012, Japan

ARTICLE INFO

Article history:
Received 2 March 2010
Revised 24 May 2010
Accepted 26 May 2010
Available online 9 June 2010

Keywords:
Fluorescence
Zinc ion
Rhodamine
Sensors

ABSTRACT

The spirolactam ring-opening process of rhodamine derivative is one of the most useful mechanisms for controlling fluorescence properties. However, the open/closed equilibrium reaction of rhodamine spirolactam has not been well characterized. Therefore, we examined the relationship between the spirolactam ring-opening process of rhodamine derivatives and the structure of the xanthene moiety. Based on the results of this investigation, we selected a candidate xanthene moiety for a Zn^{2+} sensor, and successfully developed a new fluorescence probe for Zn^{2+}.

1. Introduction

Fluorescence imaging is one of the most powerful techniques for visualization of the temporal and spatial biological events in living cells, and is employed in many fields of research. In particular, fluorescence sensor probes offer ease of use, high sensitivity, and high selectivity in visualizing biomolecules. To develop novel fluorescence sensor probes, it is important to find mechanisms for controlling fluorescence properties. For example, widely used mechanisms include Förster resonance energy transfer (FRET),[1,2] intramolecular charge transfer (ICT),[2–4] and photoinduced electron transfer (PeT).[2,5]

In the present work, we focused on the spiro-ring-opening reaction of xanthene fluorophores, such as fluorescein and rhodamine. It is well-known that the C-9 position of xanthenes shows high electrophilicity, therefore, and is readily attacked by a nucleophilic substituent on the benzene moiety, resulting in spiro-ring formation. Xanthene fluorophores in the spiro-ring configuration are colorless and non-fluorescent. This unique property can be used for fluorescence on/off switching, and indeed, has been employed in many fluorescence sensors for various biomolecules.[6–14]

There are various types of spiro-ring configurations of xanthene fluorophore, including (thio)spirolactam,[15,16] (thio)spirolactone,[6] and (thio)spirofuran.[7] Among these, we chose the spirolactam configuration of rhodamine as a good candidate for fluorescence on/off switching because of its modifiable structure. Moreover, from a chemical and biological viewpoint, rhodamine is one of the most attractive fluorescent dyes due to its excellent spectroscopic properties, such as longer wavelength (>500 nm), large molar extinction coefficient (>75,000 $cm^{-1}\,M^{-1}$), high fluorescence quantum yield, and high photostability. The development of fluorescence probes based on rhodamine spirolactam was pioneered by Czarnik et al. in 1997.[17] Since that work, many papers on fluorescence probes utilizing rhodamine spirolactam-opening, mainly for metal ions, have been reported.[18–21]

However, we thought that these probes leave room for improvement. In general, there are several important requirements for fluorescence sensor probes. Firstly, fluorescence probes for bioimaging are required to work in physiological conditions. Secondly, it is better for sensors to work reversibly, because then it is possible to examine more complex behavior of a target biomolecule. Finally, although there are many reports on fluorescence sensors utilizing the rhodamine spirolactam ring-opening process, the mechanism of fluorescence on/off switching has not been well characterized. Specifically, we investigated the influence of xanthene structure on the spirolactam ring-opening process, and utilized the results to develop a fluorescence probe for Zn^{2+}. There were two reasons for selecting Zn^{2+} as a target; one is the importance of Zn^{2+} in physiology,[22–24] and the other is that no probe based on rhodamine spirolactam has yet been developed for detecting Zn^{2+}.[25–29] Rhodamines in a spirolactam form have neither absorbance nor fluorescence in the visible region, so this kind of fluorescence probes would potentially offer a better signal-to-noise ratio in cellular applications.

* Corresponding author. Tel.: +81 3 5841 4850; fax: +81 3 5841 4855.
E-mail address: tlong@mol.f.u-tokyo.ac.jp (T. Nagano).

0968-0896/$ - see front matter © 2010 Elsevier Ltd. All rights reserved.
doi:10.1016/j.bmc.2010.05.074

2. Results and discussion

2.1. Zn^{2+} sensors based on symmetric rhodamines

Based on published reports, we hypothesized that the opening mechanism of rhodamine spirolactam upon addition of metal ions is as shown in Scheme 1.[17,19,30] Rhodamine B is mainly used as a scaffold for such fluorescence sensor probes,[9,12,18,20,21] but little is known about the effect of variation of the xanthene moiety. In other words, the relationship between the rhodamine spirolactam-opening process and the structure of the xanthene moiety of rhodamine is not been well characterized. Therefore, we designed and synthesized three candidate Zn^{2+} sensors (**5a–c**) with symmetric xanthene moieties (Fig. 1). Rhodamine 101, B, and 6G, which are commercially available, were used as xanthene moieties, and novel fluorescence sensors for Zn^{2+} (**5a–c**) were synthesized by the combination of the rhodamine derivatives (**4a–c**) and the chelator moiety, which is a ligand for Zn^{2+}. The photochemical properties in 100 mM HEPES (2-[4-(2-hydroxyethyl)-1-piperazinyl]ethanesulfonic acid) buffer (pH 7.4) of **4a–c** are shown in Table 1. Compounds **5a–c** were synthesized by treating rhodamine derivatives (**4a–c**) with $POCl_3$, followed by addition of the Zn^{2+} chelating moiety, whose carboxylic acids were protected with *tert*-butyl groups. After column chromatography using AcOEt/hexane as an eluent, the *tert*-butyl groups of products were eliminated with TFA. The products were purified by preparative HPLC in 30–50% yields. In addition, the ethyl ester of rhodamine 6G was eliminated to obtain **4c**. The synthetic schemes for **4c** and **5a–c** and details of the chemical characterization of compounds are presented in Supplementary data. Although the spirolactam configuration of rhodamine generally shows poor water solubility, the water solubility of **5a–c** was improved by incorporating two carboxylic acid groups into the Zn^{2+} chelating moiety. The improved water solubility enables us to use the probes under physiological conditions.

We assessed the spectroscopic characteristics of **5a–c** under physiological conditions (100 mM HEPES, pH 7.4; Fig. 2). The absorbance intensity changes of **5a–c** were monitored during Zn^{2+} addition (Fig. 2a). The absorbance of **5a** (10 μM) increased significantly upon addition of Zn^{2+} (0–1.0 equiv). We also measured the molar extinction coefficients (ε) of rhodamine derivatives in 100 mM HEPES buffer (pH 7.4) (Table 1); the ε value of Rho101 (**4a**) in this buffer was 116,000. This ε value was used for calculation of the fraction of open form of **5a** (=open form/(open form + closed form)) (Scheme 1), that is, when the spirolactam ring of **5a** (10 μM) is completely open, the absorbance would be 1.16. From this calculation, the fraction of open form of **5a** appeared to be over 50% under these conditions. On the other hand, the absorbance of **5b** (10 μM) or **5c** (10 μM) hardly increased upon addition of Zn^{2+} (0–1.0 equiv). The molar extinction coefficients (ε) of **4b** and **4c** in 100 mM HEPES buffer (pH 7.4) were measured by us to be 120,000 and 106,000, respectively, and the fractions of open form of **5b** and **5c** were both less than 5%.

Furthermore, we monitored the absorbance intensity changes of **5a–c** in 100 mM sodium phosphate buffer at various pH values (pH 2.0–12.0) (Fig. 2b). The absorbance of **5a** (10 μM) also increased significantly under acidic conditions. From the above ε value of **4a** in 100 mM HEPES buffer (pH 7.4), the fraction of open form of **5a** was over 50% at pH 2.0 in 100 mM sodium phosphate buffer, as was the case in the presence of Zn^{2+} (1.0 equiv). The acid dissociation constant (pK_a) of **5a**, as judged from its pH-profile, was 6.1. On the other hand, the absorbance of **5b** (10 μM) hardly increased under acidic conditions, and its pH-profile was bell-shaped. From the above ε value of **4b** in 100 mM HEPES buffer (pH 7.4), the fraction of open form of **5b** was at most 6% at pH 4.5, at which **5b** showed its absorbance maximum, in 100 mM sodium phosphate buffer. Compound **5b** has two acid dissociation constants, and the pK_{a1} and pK_{a2} of **5b** obtained from the pH-profile were 3.8 and 5.7. Further, the absorbance of **5c** (10 μM) increased remarkably under acidic conditions, and its pH-profile was bell-shaped. As judged from the above ε value of **4c** in 100 mM HEPES buffer (pH 7.4), the fraction of open form of **5c** was nearly 50% at pH 3.0, at which **5c** showed its absorbance maximum in 100 mM sodium phosphate buffer. The pK_a value of **5c** obtained from its pH-profile was 4.3.

Thus, the absorbance changes in response to Zn^{2+} addition (0–1.0 equiv) and acidic conditions (pH 2.0–7.0) were completely different among the three compounds (**5a–c**). Compound **5b** based on rhodamine B, which has been most widely used as a basic scaf-

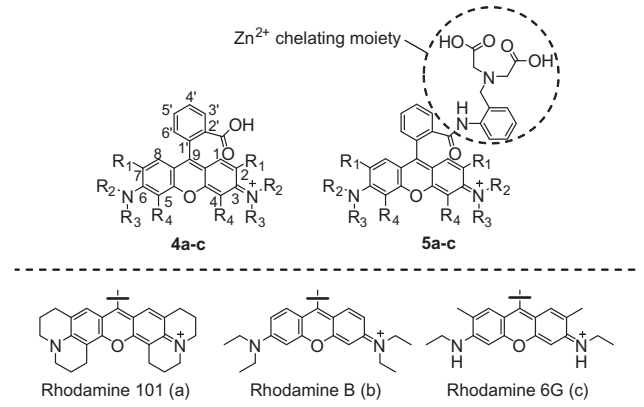

Figure 1. Structures of rhodamine derivatives **4a–c** and **5a–c**. Compounds **5a–c** were synthesized by combination of **4a–c** and a ligand for Zn^{2+}.

Table 1
Photochemical properties of **4a–c** in 100 mM HEPES buffer (pH 7.4)

Compounds	λ_{abs}[a] (nm)	λ_{em}[b] (nm)	ε[c] (cm^{-1} M^{-1})	Φ_{FL}[d]
4a	576	598	116,000	0.30
4b	554	577	120,000	0.18
4c	521	548	106,000	0.48

[a] The maximum absorption wavelengths were measured in 100 mM HEPES buffer (pH 7.4).
[b] The maximum emission wavelengths were measured in 100 mM HEPES buffer (pH 7.4).
[c] The molar extinction coefficients were measured in 100 mM HEPES buffer (pH 7.4).
[d] Fluorescence quantum efficiencies were measured in 100 mM HEPES buffer (pH 7.4) by using fluorescein in 0.1 N NaOH aq (Φ_{FL} = 0.85) as a reference.

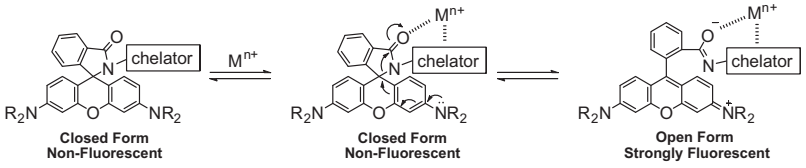

Scheme 1. Proposed mechanism of rhodamine spirolactam-opening process upon addition of a metal ion.

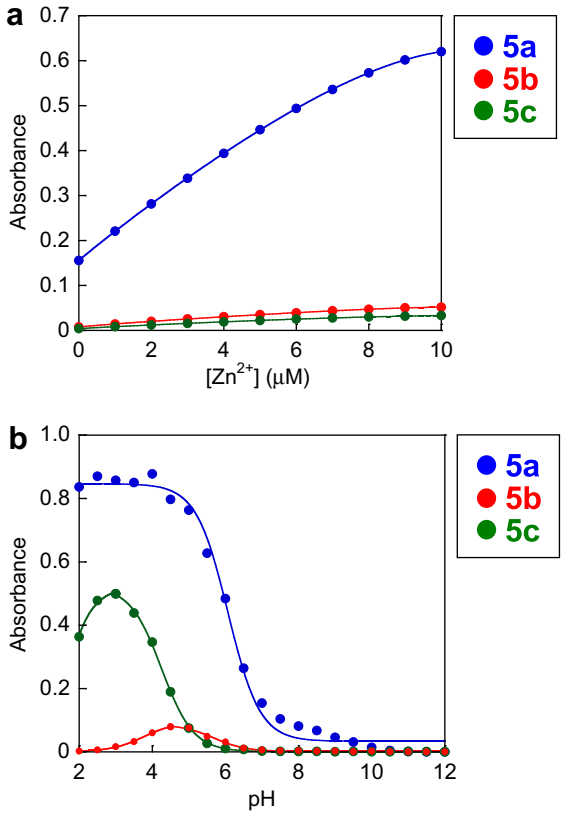

Figure 2. (a) Absorption changes of 10 μM **5a** (591 nm; blue, ●), **5b** (570 nm; red, ●), and **5c** (539 nm; green, ●) in 100 mM HEPES buffer (pH 7.4) containing 0.1% DMSO as a cosolvent in the presence of various amounts of Zn^{2+} (0–1.0 equiv). (b) Absorption changes of 10 μM **5a** (586 nm; blue, ●), **5b** (562 nm; red, ●), and **5c** (530 nm; green, ●) at various pH values (pH 2.0–12.0) in 100 mM sodium phosphate buffer containing 0.1% DMSO as a cosolvent. These samples were kept at room temperature for 2 h before measurements.

fold for fluorescence sensor probes based on rhodamine spirolactam until now, was hardly open in the presence of Zn^{2+} or under acidic conditions. On the other hand, **5a** based on rhodamine 101 showed large absorption responses to both Zn^{2+} and pH compared with **5b**. Compound **5c** based on rhodamine 6G was unique, being not quite open upon addition of Zn^{2+}, but considerably open in acid conditions. As **5a–c** have the same Zn^{2+} chelator, it is considered that the difference of responses to Zn^{2+} and pH between **5a–c** are due to the xanthene moieties of **5a–c**. We think that the xanthene substituents in **5a** preferentially stabilize the cationic open form compared with **5b** and **5c**.

Compounds **5b** and **5c** decolorized under strong acidic conditions (**5b**: pK_{a1} = 3.8, **5c**: pK_{a1} <2). A similar phenomenon was reported by Belov et al.[31] This is probably due to protonation of the N atoms of the xanthene moiety, and it is considered that this protonation led to the formation of the spirolactam-ring via nucleophilic attack of the N atom of the amide moiety on the C-9 position of the xanthene moiety.

2.2. Zn^{2+} sensors based on asymmetric rhodamines

As described above, **5a**, **5b**, and **5c** showed interesting features in the spirolactam-ring-opening reaction. However, these three rhodamine derivatives were not suitable for use as Zn^{2+} sensor, because **5a** had high background absorbance and fluorescence, while the spirolactam ring of **5b** or **5c** was hardly opened upon addition of Zn^{2+}. From these results, we expected that asymmetric rhodamine derivatives, **5d** and **5f** (Fig. 3), might have intermediate properties, that is, lower background and higher spirolactam-opening fractions in the presence of Zn^{2+}. So, we designed and synthesized asymmetric rhodamine 101/B (**4d**), rhodamine B/6G (**4e**), and rhodamine 101/6G (**4f**) (Fig. 3). The photochemical properties in 100 mM HEPES buffer (pH 7.4) of **4d–f** are shown in Table 2. Next, we synthesized asymmetric rhodamine derivatives (**5d–f**) based on **4d–f** by using the same synthetic scheme as for **5a–c** (Fig. 3). The same Zn^{2+} chelating moiety as in **5a–c** was also used for **5d–f**. The synthetic schemes for **4d–f** and **5d–f** and details of their chemical characterization are provided in the Supplementary data.

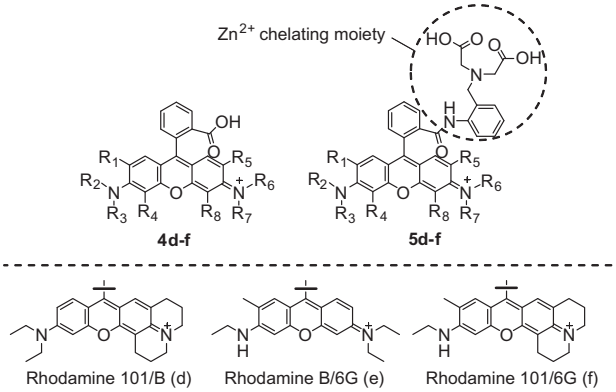

Figure 3. Structures of asymmetric rhodamine derivatives (**4d–f** and **5d–f**).

We performed spectroscopic analysis of **5d–f** under physiological conditions (100 mM HEPES, pH 7.4; Fig. 4), in the same way as for **5a–c**. The absorbance intensity changes of **5d–f** were monitored during Zn^{2+} addition. The absorbance of **5d** (10 μM) increased upon addition of Zn^{2+} (0–1.0 equiv), and its absorbance with 1.0 equiv of Zn^{2+} was intermediate between those of **5a** and **5b**. The molar extinction coefficient (ε) of **4d** in 100 mM HEPES buffer (pH 7.4) was measured to be 125,000 (Table 2), and the fraction of open form of **5d** was approximately 20% under these conditions. On the other hand, the absorbance of **5e** (10 μM) hardly increased upon addition of Zn^{2+} (0–1.0 equiv) compared with **5d** or **5f**, and its absorbance with 1.0 equiv of Zn^{2+} was intermediate between those of **5b** and **5c**. The molar extinction coefficient (ε) of **4e** in 100 mM HEPES buffer (pH 7.4) was measured to be 107,000 (Table 2), and the fraction of open form of **5e** was less than 5%. The absorbance of **5f** (10 μM) increased upon addition of Zn^{2+} (0–1.0 equiv), and its absorbance with 1.0 equiv of Zn^{2+} was intermediate between those of **5a** and **5c**. The molar extinction coefficient (ε) of **4f** in 100 mM HEPES buffer (pH 7.4) was measured to be 126,000 (Table 2), and the fraction of open form of **5f** was approximately 20%.

We also monitored the absorbance intensity changes of **5d–f** in 100 mM sodium phosphate buffer at various pH values (pH

Table 2
Photochemical properties of **4d–f** in 100 mM HEPES buffer (pH 7.4)

Compounds	λ_{abs}[a] (nm)	λ_{em}[b] (nm)	ε[c] (cm^{-1} M^{-1})	Φ_{FL}[d]
4d	566	587	125,000	0.34
4e	539	566	107,000	0.12
4f	554	580	126,000	0.32

[a] The maximum absorption wavelengths were measured in 100 mM HEPES buffer (pH 7.4).
[b] The maximum emission wavelengths were measured in 100 mM HEPES buffer (pH 7.4).
[c] The molar extinction coefficients were measured in 100 mM HEPES buffer (pH 7.4).
[d] Fluorescence quantum efficiencies were measured in 100 mM HEPES buffer (pH 7.4) by using fluorescein in 0.1 N NaOH aq (Φ_{FL} = 0.85) as a reference.

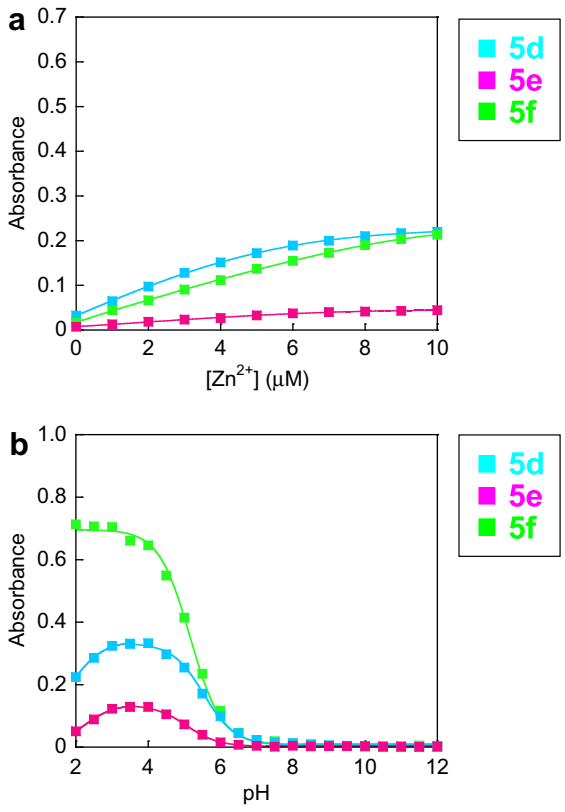

Figure 4. (a) Absorption changes of 10 μM **5d** (581 nm; light blue, ■), **5e** (557 nm; pink, ■), and **5f** (571 nm; light green, ■) in 100 mM HEPES buffer (pH 7.4) containing 0.1% DMSO as a cosolvent upon addition of various amounts of Zn^{2+} (0–1.0 equiv). (b) Absorption changes of 10 μM **5d** (574 nm; light blue, ■), **5e** (547 nm; pink, ■), and **5f** (564 nm; light green, ■) at various pH values in 100 mM sodium phosphate buffer containing 0.1% DMSO as a cosolvent. These samples were kept at room temperature for 2 h before measurements.

2.0–12.0) (Fig. 4b). The absorbance of **5d** (10 μM) increased under acidic conditions, and its pH-profile was also bell-shaped. From the above ε value of **4d** in 100 mM HEPES buffer (pH 7.4), the fraction of open form of **5d** was approximately 25% at pH 3.5, at which **5d** showed its absorbance maximum in 100 mM sodium phosphate buffer, and this fraction was intermediate between those of **5a** and **5b**. The pK_a value of **5d** obtained from its pH-profile was 5.5. On the other hand, the absorbance of **5e** (10 μM) was increased slightly compared with that of **5d** or **5f** in acidic conditions, and its pH-profile was bell-shaped. From the above ε value of **4e** in 100 mM HEPES buffer (pH 7.4), the fraction of open form of **5e** was around 12% at pH 3.5, at which **5e** showed its maximum absorbance in 100 mM sodium phosphate buffer. This fraction of **5e** was intermediate between those of **5b** and **5c**. Compound **5e** has two acid dissociation constants, and pK_{a1} and pK_{a2} of **5e** obtained from its pH-profile were 2.2 and 5.1. Further, the absorbance of **5f** (10 μM) was increased significantly compared with that of **5e** under acidic conditions. From the above ε value of **4f** in 100 mM HEPES buffer (pH 7.4), the fraction of open form of **5f** was over 50% at pH 2.0. This fraction of **5f** was intermediate between those of **5a** and **5c**, and the pK_a value of **5f** obtained from its pH-profile was 5.2.

The spirolactam-ring-opening processes in response to Zn^{2+} (0–1.0 equiv) and pH (2.0–12.0) of the above three asymmetric compounds (**5d–f**) had the intermediate properties between those of symmetric rhodamine derivatives (**5a–c**). In particular, **5d** based on **4a** and **4b**, and **5f** based on **4a** and **4c**, both had lower background compared with **5a**, and their fractions of open form were larger than that of **5b** or **5c** upon addition of Zn^{2+}, as we had expected. The pK_a values of **5d–f** also basically lay in the middle of those of **5a–c**.

2.3. Fluorescence and chemical properties of 5f

Among **5a–f**, **5f** is the most suitable compound for use as a Zn^{2+} sensor because of its approximately 12-fold enhancement in both absorbance at 571 nm and fluorescence intensity at 595 nm; this enhancement is the largest among the six compounds (**5a–f**) (Table S2 and Fig. S3, Supplementary data). Therefore, we chose **5f** as a fluorescence probe for Zn^{2+}, and its photochemical properties in the presence of Zn^{2+} were examined in detail. The UV–vis absorption and fluorescence emission spectral changes of **5f** (10 μM) during Zn^{2+} addition (0–1.0 equiv) in 100 mM HEPES buffer (pH 7.4) are shown in Figure 5. Compound **5f** displayed a major absorption band centered at λ = 571 nm, and the fluorescence emission spectrum of **5f** had a major band at 595 nm. The fluorescence emission intensity of **5f** remained almost at a plateau level in the presence of an excess of Zn^{2+} (the inset of Fig. 5b). Compound **5f** achieved equilibrium between open and closed forms upon addition of Zn^{2+} within 30 s (Fig. S7, Supplementary data). Photographs of absorbance and fluorescence of a solution of **5f** (the inset of Fig. 5a and b) show the marked color change between without Zn^{2+} and with Zn^{2+} (1.0 equiv). Further, the Job's plot of the absorbance of **5f** at 571 nm indicates that the coordination of **5f** with Zn^{2+} occurs

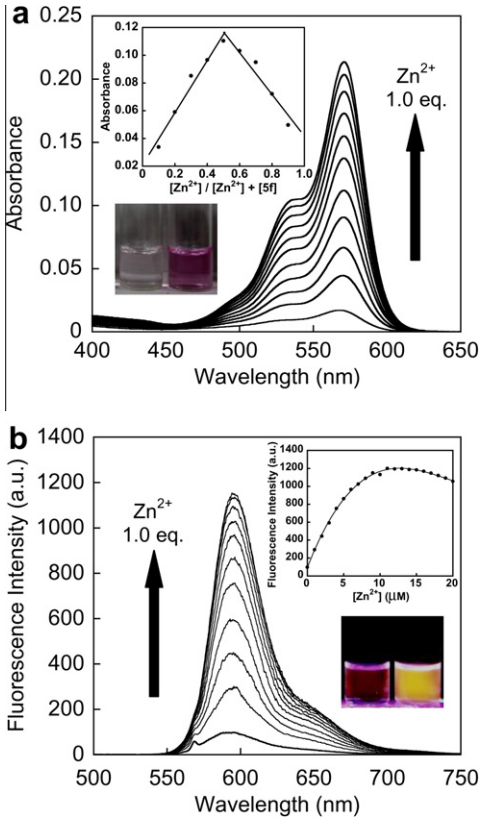

Figure 5. (a) Absorption spectra of **5f** (10 μM) in 100 mM HEPES buffer (pH 7.4) in the presence of various amounts of Zn^{2+} (0–1.0 equiv). Inset: the Job's plot; the total concentration of ([Zn^{2+}] + [**5f**]) was 10 μM. The photograph shows the color change of **5f** (10 μM) upon addition of Zn^{2+} (0 equiv or 1.0 equiv) in 100 mM HEPES buffer (pH 7.4). (b) Fluorescence emission spectra of **5f** (10 μM) in 100 mM HEPES buffer (pH 7.4) with various amounts of Zn^{2+} (0–1.0 equiv). The excitation wavelength was 565 nm. Inset: fluorescence intensities at 595 nm of **5f** (10 μM) with various amounts of Zn^{2+} (0–2.0 equiv). The photograph shows the fluorescence color of **5f** (10 μM) upon addition of Zn^{2+} (0 equiv or 1.0 equiv) in 100 mM HEPES buffer (pH 7.4) with 365 nm excitation.

to form a 1:1 complex (the inset of Fig. 5a). The apparent dissociation constant K_d of **5f** for Zn^{2+} was calculated to be 4.1 μM from the Zn^{2+} titration curves of fluorescence intensity at 594 nm (Fig. S4, Supplementary data), and this K_d value is sufficiently small for biological applications.[23] The values of fluorescence quantum efficiency (Φ_{FL}) of **5f** measured with fluorescein in 0.1 N NaOH aq (Φ_{FL} = 0.85) as a reference were 0.13 in the presence of Zn^{2+} (1.0 equiv with respect to **5f**) in 100 mM HEPES buffer (pH 7.4) and 0.28 in 100 mM sodium phosphate buffer (pH 2.0) (Table S3, Supplementary data). In addition, we added an aqueous solution of ethylenediamine-*N*,*N*,*N*′,*N*′-tetraacetic acid, disodium salt (EDTA·2Na) to **5f** (10 μM) with 1.0 equiv of Zn^{2+} in 100 mM HEPES buffer (pH 7.4) to examine the reversibility of complex formation of **5f** and Zn^{2+} (Table S4 and Fig. S5, Supplementary data). When EDTA (1.0 equiv with respect to **5f**) was added to the solution, the color of solution changed from purple to colorless. Next, when Zn^{2+} (1.0 equiv with respect to **5f**) was further added to the solution, the purple color was recovered. This result indicated that **5f** could work as a reversible chemosensor for Zn^{2+}.

Furthermore, the effect of adding various heavy metal ions (1.0 equiv with respect to **5f**), Ca^{2+} (5 mM), Mg^{2+} (5 mM), Na^{+} (100 mM), and K^{+} (100 mM) on the absorbance and the fluorescence intensity of **5f** was examined in 100 mM HEPES buffer (pH 7.4) (Fig. 6 and Fig. S6, Supplementary data). Absorbance change of **5f** (10 μM) was observed upon addition of Zn^{2+}, Ni^{2+},Co^{2+}, or Cu^{2+} (1.0 equiv with respect to **5f**) (Fig. S6ab, Supplementary data).

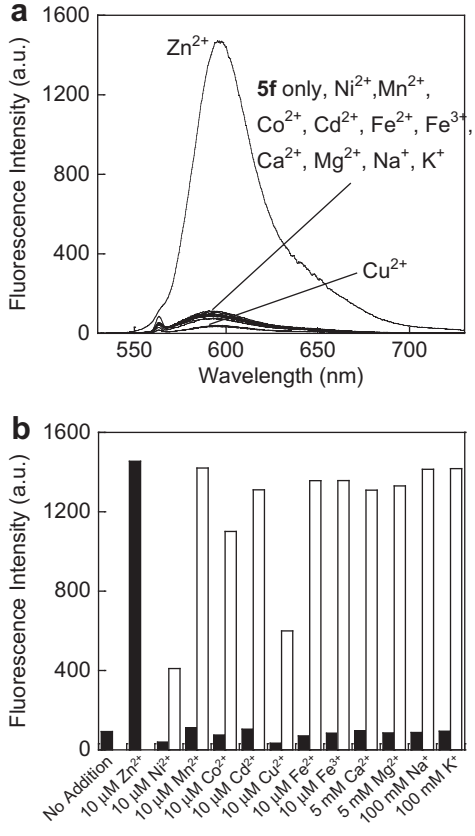

Figure 6. (a) Fluorescence emission spectra of **5f** (10 μM) in the presence of various cations. (b) Bars indicate the fluorescence intensities of **5f** (10 μM) aqueous solution at 594 nm in the presence of various cations. Colored bars: each cation was added. Colorless bars: each cation was added in the presence of Zn^{2+} (10 μM). Heavy metal ions (1.0 equiv. with respect to **5f**) were added as $NiSO_4$, $MnSO_4$, $CoSO_4$, $CdSO_4$, $CuSO_4$, $FeCl_2$, and $FeCl_3$. Other cations were added as $ZnSO_4$ (10 μM), $CaCl_2$ (5 mM), $MgSO_4$ (5 mM), $NaNO_3$ (100 mM), and KNO_3 (100 mM). All samples were measured in 100 mM HEPES buffer (pH 7.4) with 565 nm excitation.

On the other hand, fluorescence emission enhancement of **5f** (10 μM) was observed only upon addition of Zn^{2+}, showing high selectivity for Zn^{2+} (Fig. 6a and Fig. S6c, Supplementary data). The fluorescence intensity of **5f** was weakened by the addition of several cations (particularly Ni^{2+}, Cu^{2+}, and Co^{2+}) together with Zn^{2+}, in comparison with that upon addition of Zn^{2+} alone (Fig. 6b). However, Zn^{2+} can be distinguished from those heavy metals, since only Zn^{2+} chelation enhances the fluorescence intensity. In addition, although Zn^{2+} sensors generally show poor selectivity between Zn^{2+} and Cd^{2+}, **5f** did not show any fluorescence enhancement upon addition of Cd^{2+}. The equilibrium of **5f** between open and closed forms upon addition of Cd^{2+} also did not change for at least 10 min (Fig. S7, Supplementary data). Moreover, Ca^{2+}, Mg^{2+}, Na^{+}, and K^{+}, which exist at high concentrations in living cells, also did not enhance the fluorescence intensity of **5f** (Fig. 6 and Fig. S6, Supplementary data). These results indicate that **5f** has high selectivity for Zn^{2+} over various cations, especially those likely to be encountered in biological applications.

3. Conclusion

In conclusion, we anticipated that the open/closed equilibrium reaction of rhodamine spirolactam would be profoundly influenced by the xanthene structure of rhodamine derivatives. Therefore, we designed and synthesized a series of Zn^{2+} sensors based on symmetric or asymmetric rhodamine derivatives (**5a–f**), and examined the changes of their absorbance and fluorescence spectra in response to ring-opening induced by Zn^{2+}.

We selected the rhodamine derivative **5f** as a candidate fluorescence probe for Zn^{2+}, on the basis of the above results, and confirmed that **5f** could selectively recognize Zn^{2+} in physiological solution in terms of fluorescence responses. In addition, the Job's plot showed that **5f** formed a 1:1 complex with Zn^{2+}, and the reversibility of the reaction of **5f** with Zn^{2+} was confirmed by treatment with EDTA followed by further addition of Zn^{2+}. Compound **5f** also showed high selectivity over various cations, including Cd^{2+}, which most Zn^{2+} sensor probes are unable to distinguish from Zn^{2+}. There have been many reports of rhodamine-based on/off fluorescence sensor molecules for various cations, such as Hg^{2+}, Cu^{2+}, and Fe^{3+}, by using the spirolactam-ring-opening process. However, compound **5f** is the first Zn^{2+}-selective fluorescence sensor molecule based on the spirolactam-ring-opening process of rhodamines. We believe our design strategy for the rhodamine spirolactam-ring has great potential for further development of excellent fluorescence probes, and could be applied to develop fluorescence sensors for other molecules of interest in biological applications.

4. Experimental

4.1. Materials

All reagents and solvents were of the best commercial grade, supplied by Tokyo Chemical Industry Co. Ltd (Tokyo, Japan), Wako Pure Chemical Industries, Ltd (Osaka, Japan), or Aldrich Chemical Co. Inc. (Milwaukee, WI), and were used without further purification. Rhodamine 101 was purchased from Acros Organics (Geel, Belgium). Rhodamine B and rhodamine 6G were purchased from Tokyo Chemical Industry Co, Ltd (Tokyo, Japan). All other rhodamines were prepared as described in the Supplementary data. Water (H_2O, fluorometric grade), dimethyl sulfoxide (DMSO, fluorometric grade), dimethyl formamide (DMF, fluorometric grade), methyl alcohol (MeOH, fluorometric grade), acetonitrile (CH_3CN, fluorometric grade), acetone (fluorometric grade), methylene chloride (CH_2Cl_2, fluorometric grade), chloroform ($CHCl_3$, fluorometric

grade), tetrahydrofuran (THF, fluorometric grade), toluene (fluorometric grade), benzene (fluorometric grade), 2-[4-(2-hydroxymethyl)-1-piperazinyl]ethanesulfonic acid (HEPES), and ethylenediamine-*N*,*N*,*N*′,*N*′-tetraacetic acid, disodium salt, dehydrate (EDTA·2Na) used for spectrometric measurements were purchased from Dojindo (Kumamoto, Japan). Silica gel column chromatography was performed using Chromatorex-NH (Fuji Silysia Chemical Ltd, Aichi, Japan), Silica Gel 60 (Kanto Chemical Co. Inc., Tokyo, Japan), or Silica Gel 60 N (Kanto Chemical Co. Inc., Tokyo, Japan).

4.2. Instruments and general methods

HPLC preparation or analysis was performed on a reverse-phase column (Inertsil ODS-3 10 mm × 250 mm for purification and Inertsil ODS-3 4.6 × 250 mm for analysis; GL Sciences (Tokyo, Japan)) using eluent A (H_2O containing 0.1% TFA (v/v)) and eluent B (CH_3CN with 20% H_2O containing 0.1% TFA (v/v)), fitted on a Jasco PU-2080 system. NMR spectra were recorded on a JNM-LA300 or JNM-LA400 (JEOL Ltd, Tokyo, Japan) instrument at 300 MHz or 400 MHz for ^1H NMR and at 75 MHz or 100 MHz for ^{13}C NMR, respectively. Mass spectra (MS) were measured with a JEOL JMS-T100LC AccuTOF mass spectrometer (ESI^+ or ESI^-).

4.3. Measurements of photochemical properties

Absorption spectra were obtained with a UV–vis spectrometer UV-1650 (Shimadzu Corp., Kyoto, Japan). Fluorescence spectroscopic studies were performed with a F-4500 Hitachi fluorescence spectrophotometer (Hitachi, Ltd, Tokyo, Japan). The slit width was 2.5 nm for both excitation and emission. The photomultiplier voltage was 700 V. All experiments were carried out at 25 °C. Photochemical properties of dyes were examined in 100 mM HEPES buffer (pH 7.4) or 100 mM sodium phosphate buffer (pH 2.0–12.0) containing less than 1% (v/v) DMSO as a cosolvent. Values of relative quantum efficiency of fluorescence (Φ_{FL}) were determined based on fluorescein in 0.1 N NaOH aq ($\Phi_{FL} = 0.85$) as a standard, using the following equation:

$$\Phi_x/\Phi_{std} = [A_{std}/A_x][n_x^2/n_{std}^2][D_x/D_{std}]$$

where std, standard, *x*, sample; *A*, absorbance at the excitation wavelength; *n*, refractive index; *D*, area under the fluorescence spectra on an energy scale.

4.4. Apparent dissociation constant (K_d) measurements

We prepared 100 mM HEPES buffer (pH 7.4, $I = 0.1$ ($NaNO_3$)) containing 10 mM iminodiacetic acid (IDA) and 0–9.7 mM $ZnSO_4$. The stability constant of IDA for Zn^{2+} was reported in Ref. 32. For IDA,

$$pK_{a1} = 9.33,\ pK_{a2} = 2.58,\ \log K(\mathrm{ZnL}) = 7.27$$

Protonation constants must be corrected upward by 0.11 when working in 0.1 M ionic strength. Using these values, free Zn^{2+} concentration was calculated according to the method described in Ref. 33, as follows:

$$[Zn^{2+}]_{free} = [Zn^{2+}]_{total}/K(\mathrm{ZnL}) \times \alpha_M \times [L]_{free} \quad (1)$$

$$\alpha_M = 1 + 10^{(pH - pK_{a1})} + 10^{(2pH - pK_{a2})}$$

$$[L]_{free} = [L]_{total} - [Zn^{2+}]_{total}$$

$[L]_{total}$ was 10 mM, and $[Zn^{2+}]_{total}$ was varied from 0 to 9.7 mM.

The value of $[Zn^{2+}]_{free}$ was obtained from Eq. 1.

$[Zn^{2+}]_{total}$ (mM): 0.085, 0.21, 0.33, 0.80, 1.2, 3.5, 4.6, 5.8, 6.8, 7.7, 8.4, 9.0, 9.3, 9.6, 9.7.

$[Zn^{2+}]_{free}$ (μM): 0.040, 0.10, 0.16, 0.40, 0.63, 2.5, 4.0, 6.3, 10, 16, 25, 40, 63, 100, 160.

4.5. Metal ion selectivity measurements

The absorption and the fluorescence emission enhancement of **5f** were measured in 100 mM HEPES buffer (pH 7.4) (excitation 565 nm). Heavy metals (10 μM) were added as $NiSO_4$, $MnSO_4$, $CoSO_4$, $CdSO_4$, $CuSO_4$, $FeCl_2$, and $FeCl_3$. Other cations were added as $ZnSO_4$ (10 μM), $CaCl_2$ (5 mM), $MgSO_4$ (5 mM), $NaNO_3$ (100 mM), and KNO_3 (100 mM).

Acknowledgments

This work was supported in part by the Ministry of Education, Culture, Sports, Science and Technology of the Japan (Grant Nos. 20689001, 19890047 and 21659024 to K.H., 19205021 and 20117003 to Y.U., and 21750135 to T.T.), and by a grant from the Industrial Technology Development Organization (NEDO) of Japan (to T.T.). K.H. was also supported by The Mochida Memorial Foundation for Medical Pharmaceutical Research, and Sankyo Foundation of Life Science.

Supplementary data

Supplementary data associated with this article can be found, in the online version, at doi:10.1016/j.bmc.2010.05.074.

References and notes

1. Takakusa, H.; Kikuchi, K.; Urano, Y.; Kojima, H.; Nagano, T. *Chem. Eur. J.* **2003**, *9*, 1479.
2. de Silva, A. P.; Gunaratne, H. Q. N.; Gunnlaugsson, T.; Huxley, A. J. M.; McCoy, C. P.; Rademacher, J. T.; Rice, T. E. *Chem. Rev.* **1997**, *97*, 1515.
3. Maruyama, S.; Kikuchi, K.; Hirano, T.; Urano, Y.; Nagano, T. *J. Am. Chem. Soc.* **2002**, *124*, 10650.
4. Mizukami, S.; Nagano, T.; Urano, Y.; Odani, A.; Kikuchi, K. *J. Am. Chem. Soc.* **2002**, *124*, 3920.
5. Gabe, Y.; Urano, Y.; Kikuchi, K.; Kojima, H.; Nagano, T. *J. Am. Chem. Soc.* **2004**, *126*, 3357.
6. Pires, M. M.; Chmielewski, J. *Org. Lett.* **2008**, *10*, 837.
7. Kenmoku, S.; Urano, Y.; Kojima, H.; Nagano, T. *J. Am. Chem. Soc.* **2007**, *129*, 7313.
8. Wu, J. S.; Kim, H. J.; Lee, M. H.; Yoon, J. H.; Lee, J. H.; Kim, J. S. *Tetrahedron Lett.* **2007**, *48*, 3159.
9. Zheng, H.; Shang, G. Q.; Yang, S. Y.; Gao, X.; Xu, J. G. *Org. Lett.* **2008**, *10*, 2357.
10. Franzini, R. M.; Kool, E. T. *Org. Lett.* **2008**, *10*, 2935.
11. Zhang, W. S.; Tang, B.; Liu, X.; Liu, Y. Y.; Xu, K. H.; Ma, J. P.; Tong, L. L.; Yang, G. W. *Analyst* **2009**, *134*, 367.
12. Huang, K.; Yang, H.; Zhou, Z.; Yu, M.; Li, F.; Gao, X.; Yi, T.; Huang, C. *Org. Lett.* **2008**, *10*, 2557.
13. Jou, M. J.; Chen, X.; Swamy, K. M.; Kim, H. N.; Kim, H. J.; Lee, S. G.; Yoon, J. *Chem. Commun.* **2009**, 7218.
14. Chatterjee, A.; Santra, M.; Won, N.; Kim, S.; Kim, J. K.; Kim, S. B.; Ahn, K. H. *J. Am. Chem. Soc.* **2009**, *131*, 2040.
15. Yang, X. F.; Liu, P.; Wang, L.; Zhao, M. *J. Fluoresc.* **2008**, *18*, 453.
16. Liu, W.; Xu, L.; Zhang, H.; You, J.; Zhang, X.; Sheng, R.; Li, H.; Wu, S.; Wang, P. *Org. Biomol. Chem.* **2009**, *7*, 660.
17. Dujols, V.; Ford, F.; Czarnik, A. W. *J. Am. Chem. Soc.* **1997**, *119*, 7386.
18. Huang, J.; Xu, Y.; Qian, X. *J. Org. Chem.* **2009**, *74*, 2167.
19. Yang, Y. K.; Yook, K. J.; Tae, J. *J. Am. Chem. Soc.* **2005**, *127*, 16760.
20. Zhang, M.; Gao, Y. H.; Li, M. Y.; Yu, M. X.; Li, F. Y.; Li, L.; Zhu, M. W.; Zhang, J. P.; Yi, T.; Huang, C. H. *Tetrahedron Lett.* **2007**, *48*, 3709.
21. Kwon, J. Y.; Jang, Y. J.; Lee, Y. J.; Kim, K. M.; Seo, M. S.; Nam, W.; Yoon, J. *J. Am. Chem. Soc.* **2005**, *127*, 10107.
22. Domaille, D. W.; Que, E. L.; Chang, C. J. *Nat. Chem. Biol.* **2008**, *4*, 168.
23. Jiang, P.; Guo, Z. *Coord. Chem. Rev.* **2004**, *248*, 205.
24. Que, E. L.; Domaille, D. W.; Chang, C. J. *Chem. Rev.* **2008**, *108*, 1517.
25. Woodroofe, C. C.; Lippard, S. J. *J. Am. Chem. Soc.* **2003**, *125*, 11458.
26. Hirano, T.; Kikuchi, K.; Urano, Y.; Nagano, T. *J. Am. Chem. Soc.* **2002**, *124*, 6555.
27. Gee, K. R.; Zhou, Z. L.; Ton-That, D.; Sensi, S. L.; Weiss, J. H. *Cell Calcium* **2002**, *31*, 245.

28. Hanaoka, K.; Kikuchi, K.; Kojima, H.; Urano, Y.; Nagano, T. *Angew. Chem., Int. Ed.* **2003**, *42*, 2996.
29. Taki, M.; Wolford, J. L.; O'Halloran, T. V. *J. Am. Chem. Soc.* **2004**, *126*, 712.
30. Chen, X. Q.; Jia, J.; Ma, H. M.; Wang, S. J.; Wang, X. C. *Anal. Chim. Acta* **2009**, *632*, 9.
31. Belov, V. N.; Bossi, M. L.; Folling, J.; Boyarskiy, V. P.; Hell, S. W. *Chem. Eur. J.* **2009**, *15*, 10762.
32. Dojindo Catalogue 25th ed., 2006/2007.
33. Fahrni, C. J.; O'Halloran, T. V. *J. Am. Chem. Soc.* **1999**, *121*, 11448.